Journal of the European Ceramic Society 42 (2022) 5943–5952

Contents lists available at ScienceDirect

Journal of the European Ceramic Society

journal homepage: www.elsevier.com/locate/jeurceramsoc

Highly efficient electrical discharge machining of yttria-stabilized zirconia ceramics with graphene nanostructures as fillers

C. Muñoz-Ferreiro [a,b,c], C. López-Pernía [a], R. Moriche [a], A. Gommeringer [d], F. Kern [d], R. Poyato [c], Á. Gallardo-López [a,*]

[a] Dept. de Física de la Materia Condensada, ICMS, CSIC-Universidad de Sevilla, Apdo. 1065, 41080 Sevilla, Spain
[b] Université de Lyon, INSA Lyon, MATEIS UMR CNRS 5510, 7 Avenue Jean Capelle, F-69621 Villeurbanne Cedex, France
[c] Inst. Ciencia de Materiales de Sevilla, ICMS, CSIC-Universidad de Sevilla, Américo Vespucio 49, 41092 Sevilla, Spain
[d] Institute for Manufacturing Technologies of Ceramic Components and Composites (IFKB), University of Stuttgart, Allmandring 7b, D-70569 Stuttgart, Germany

ARTICLE INFO

Keywords:
Electrical discharge machining (EDM)
Zirconia
Graphene-ceramic composites
Surface roughness
Scanning electron microscopy

ABSTRACT

Electrical-discharge machining (EDM) of advanced ceramics allows the miniaturization of parts with complex shapes. Since electrical conductivity is required, non-conductive ceramics need a conductive second phase. This work assesses the feasibility of industrial EDM in advanced yttria-stabilized tetragonal zirconia (3YTZP) composites with 20 vol% graphene nanostructures with different morphology using different EDM energies. The structural integrity of the graphene nanostructures, the roughness of the machined surfaces and the geometrical tolerances have been evaluated by Raman spectroscopy, confocal microscopy and scanning electron microscopy, showing that it is possible to obtain a stable and efficient EDM process in these composites using low electrode energies. The use of the largest and thickest graphene nanostructures led to the best performance in terms of EDM machinability, the smallest nanostructures produced the best surface finish for low electrode energy and the thinnest nanostructures allowed the highest material removal rate at medium energy in the composites.

1. Introduction

Thanks to their elevated values of hardness, resistance to temperature and wear, chemical stability and biocompatibility, structural ceramic materials are commonly used in a wide variety of applications in the aeronautical, aerospace and biomedical industries. However, one of the major drawbacks in the use of ceramics in these sectors is the high cost and complexity of their machining, especially to obtain micro-parts, as a consequence of their high hardness and brittleness. While conventional mechanical machining techniques show major drawbacks such as high tool wear, long processes and high costs, chemical machining techniques have also serious drawbacks such as the possibility of associated environmental risk due to the waste generated during the process [1,2].

In this context, the search for techniques that allow the erosion of the material - and finally the manufacture of micro-parts with highly precise complex shapes - without compromising the properties of the material and in an economical and eco-sustainable way is one of the major challenges in the area of ceramic materials.

Among the processes known as "non-contact" machining, the electrical discharge machining (EDM) stands out. This technique, commonly used for metal machining, has revolutionized the ceramic machining process due to the particular mechanisms generated to erode the material. It consists of an electro-thermal process that uses the electrical energy from a discharge to erode the material, being independent of its hardness. Additionally, EDM has a low environmental impact, which makes it an ideal technique for manufacture industries to adapt to the ISO 14,000 standard for environmental management [2]. However, this technique requires materials with a certain electrical conductivity, so its use for the machining of ceramics, mostly non-conductive, is still very limited and poses an interesting scientific and technological challenge. Although alternative techniques with an assisting electrode, AEM (Assisting Electrode Machining) have been explored for these non-conductive ceramics, they present disadvantages such as lower process stability and lower material removal rates, and their use is mainly limited to a laboratory scale [1].

One of the approaches used to confer electrical conductivity to structural ceramics is the introduction of a conductive second phase,

* Corresponding author.
E-mail address: angela@us.es (Á. Gallardo-López).

https://doi.org/10.1016/j.jeurceramsoc.2022.06.037
Received 28 January 2022; Received in revised form 7 June 2022; Accepted 11 June 2022
Available online 14 June 2022

usually in the form of micro or nanoparticles of transition metal carbides, nitrides or borides, to matrices of alumina, zirconia, silicon nitride or silicon carbide. Some of these materials are already patented or can be purchased commercially with sufficient conductivity for EDM [3].

Tetragonal zirconia is an advanced ceramic with exceptional mechanical properties such as high fracture toughness and mechanical resistance, as well as high biocompatibility. In the specific case of this ceramic, EDM studies have been published with promising results with the introduction of NbC, TiN or WC particles [3–5].

In recent years, carbon nanostructures - carbon nanotubes (CNT) or graphene nanoplatelets (GNP) - have been approached as conductive second phase to allow the ED-machinability of ceramics, given the exceptional electrical conductivity presented by these nanomaterials. In the case of carbon nanotubes, a few studies have been published on composites with alumina [6], zirconia [7] and silicon nitride [8] matrices. Even the manufacture of a micro gear from a composite of silicon nitride with multilayer carbon nanotubes has been achieved [9]. Recently, promising results have also been published in alumina, silicon carbide and boron carbide composites with GNP [10–12]. However, to our knowledge, there is only one published work in which the EDM of zirconia composites with graphene nanoplatelets has been addressed, without achieving the desired results [13]. There is also a lack of systematic studies on the influence of the graphene nanoplatelets features (such as dimensions or number of layers) or the influence of the processing route on the ED machinability of the resulting GNP ceramic composites.

This work reports the efficient ED-machining of zirconia ceramic composites with different graphene based-nanomaterials (GBN) using a conventional industrial EDM equipment, by the die-sinking technique. Spark plasma sintered yttria tetragonal zirconia polycrystalline (3YTZP) composites with 20 vol% different graphene nanostructures: (i) low-cost GNP, ii) exfoliated GNP and iii) few layered graphene (FLG), have been EDMed with different energy parameters. The best conditions for a high EDM efficiency are assessed in terms of the material removal rate (MRR) and by the analysis of significant surface finish parameters such as angular tolerance, roughness, carbon nanostructures' integrity, surface composition and the microstructural material removal mechanisms.

2. Materials and methods

2.1. Composite fabrication

3YTZP powder with 40 nm particle size, ref. TZ-3YB-E, supplied by Tosoh Europe (Amsterdam, Netherlands) was annealed at 850 °C for 30 min in air and then it was mixed with 20 vol% graphene-based nanomaterials. The GBN used in this work were graphene nanoplatelets, with more than 10 graphene layers, less than 5 μm planar diameter and 10–20 nm thickness supplied by Angstron Materials (Dayton, Ohio, USA) and few layer graphene, with less than 5 graphene layers and a specific surface area of 400 mm^2/gm, supplied by Grolman Iberia S.L. (Barcelona, Spain). Three different composites were fabricated:

i) GNP composite. The GNP were mixed with the ceramic powder in isopropyl alcohol using ultrasonic agitation probe, and the composite powder was sintered by spark plasma at 1250 °C as described in a previous work [14].
ii) e-GNP composite. The GNP were mixed with the ceramic powder by planetary ball milling (PBM) in dry conditions, and the composite powder was SPSed at 1250 °C as described in a previous work [15]. The high-energy milling process breaks and exfoliates the GNP, so they are referred as exfoliated GNP (e-GNP).
iii) FLG composite. The FLG were mixed with the ceramic powder in isopropyl alcohol using an ultrasonic bath, as detailed in a previous work and the composite powder was SPSed at 1300 °C. The higher sintering temperature was chosen to obtain composites with higher electrical conductivity [16].

The resulting dense composites were discs with 15 mm diameter and ~3 mm thickness. The density of the composites was measured by the Archimedes' method, according to the ASTM International Standard B 311–93/02: "Test Method for Density Determination for Powder Metallurgy (PM)". The theoretical density was calculated using a GBN density of 2.2 g/cm^3 and a 3YTZP density of 6.05 g/cm^3.

2.2. Microstructural and electrical characterization of the as-sintered composites

The different as-sintered microstructures, emphasizing the different GBN size and distribution are shown in Fig. 1, where polished cross sections of the three composites are imaged. The dark areas correspond to the GBN phases while the light areas show the 3YTZP matrix. The GBN arrange themselves surrounding areas comprising several ceramic grains, and do not usually surround individual grains. The ceramic grain boundaries cannot be distinguished in these micrographs. While the e-GNP are the smallest GBN and produce the most homogeneous composite, the GNP are the largest structures and the corresponding composites show the largest oval GBN-free ceramic areas. Further comparative microstructural aspects and additional micrographs can be consulted in previous works [14–17].

To estimate the grain size of the ceramic matrix, cross section surfaces of the composites were polished with diamond paste up to 1 μm, annealed for 15 min in air at a temperature 100 ºC lower than the composite sintering temperature, and analyzed by low magnification conventional scanning electron microscopy (SEM, FEI-Teneo, FEI, USA, Centro de Investigación, Tecnología e Innovación de la Universidad de Sevilla, CITIUS). The equivalent planar diameter, $d = 2(\text{area}/\pi)^{1/2}$, namely the diameter corresponding to a circle with the same area as the measured grain, was taken as a measure of the ceramic grain size. The shape factor of the grains was calculated as $F = 4\pi\ \text{area}/(\text{perimeter})^2$. The ImageJ and Origin software were used to quantify these morphological parameters, averaging 200–300 grains, according to UNE-EN ISO 13383–1:2016 standard.

In order to estimate the electrical conductivity, the samples were cut into parallelepipedic specimens, two parallel faces were coated with colloidal silver paste, and the electrodes were fired at 600 ºC for 30 min under Ar flow to avoid any degradation of the GBN during the process. The measurements were performed at room temperature in a four-point configuration with a Solartron SI 1260 A (Ametek Scientific Instruments, Berwyn, PA, USA, CITIUS) using a potentiodynamic method with a 0–10 mV range in steps of 1 mV. In order to account for any degree of electrical anisotropy in the composites, two different electrode configurations were used to obtain the electrical conductivity in the directions parallel ($\sigma_{//}$) and perpendicular ($\sigma_{\perp}$) to the compression axis during SPS.

2.3. EDM tests

The ED-machining tests were performed by a die sinking machine (AEG Elotherm, Germany) with oil-based dielectric and copper electrodes. This machine operates with fixed parameters, not allowing self-optimization algorithm. Three different energies (discharge current levels) measured in situ with a measuring clamp (ILA SMZ 200, University of Stuttgart, Germany) coupled to an oscilloscope (DS4022, RIGOL Technologies, Inc., China) were tested on the composites. The experimental eroding conditions: discharge current, pulse duration and time lapse between pulses for each experiment are summarized in Table 1. The material removal rate (MRR) was calculated from the weight loss of the sample after machining a rectangular 3×5 mm^2 cavity for 15 min. The corresponding weight loss of the electrode was also measured to determine electrode wear. The electrodes were applied to the external curved surface of the cylinder-shaped samples, in the radial direction, as can be seen in Fig. 1.

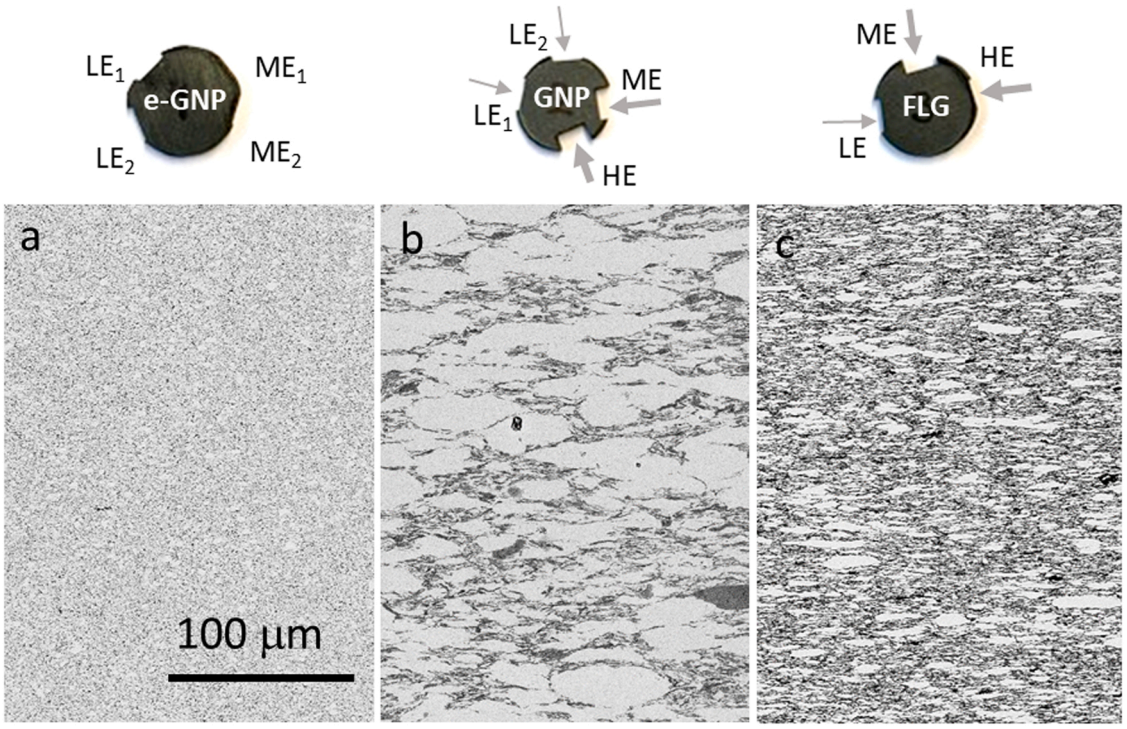

Fig. 1. Pictures of the three EDMed composites with rectangular electrodes' imprints at different electrode energies (low energy LE, medium ME and high HE) and the corresponding SEM-BSE micrographs showing the graphene nanostructures' distribution (dark phase) in the 3YTZP matrix (light phase) in each composite (cross sections). (a) e-GNP composite, with exfoliated nanostuctures, (b) composite with largest graphene nanoplatelets, GNP and (c) composite with the thinnest nanostructures, few layer graphene or FLG.

Table 1
Experimental EDM eroding parameters. LE, ME and HE stand for low, medium and high energy, respectively, regarding the discharge current.

Material	Energy	Experiment code	Discharge Current [A]	Pulse duration [µs]	Time lapse between pulses [µs]
e-GNP	Low	1-LE	3.5	8	35
		2-LE	3.5	8	30
	Medium	1-ME	~ 6.4	~ 16	_
		2-ME	~ 6.4	~ 16	_
GNP	Low	1-LE	3.5	7	40
		2-LE	3.5	8	40
	Medium	1-ME	6.4	15	35
	High	1-HE	9.4	20	35
FLG	Low	1-LE	3.3	7	40
	Medium	1-ME	6.5	14	35
	High	1-HE	~ 9	_	_

2.4. Microstructural characterization of the EDMed surfaces

The microstructure of the EDMed surfaces was analyzed by different techniques. Confocal microscopy (DM3D, Leica, Germany) was used to estimate the tolerances and the surface roughness. Raman spectroscopy (3–4 spectra acquired from each eroded surface) was used to evaluate the integrity of the graphene nanostructures after the EDM process. The equipment was a spectrometer Raman Horiba Jobin Yvon LabRaman HR800 with Olympus BX 41optic system and Labsec 5.25.15 data acquisition software (Instituto de Ciencia de Materiales de Sevilla, ICMS), using a 20 mW power green He-Ne laser (532.1 nm), a diffraction grid of 600 lines/mm and a 100x objective with 100 µm confocal aperture. Finally, scanning electron microscopy, SEM,) and energy-dispersive X-ray spectroscopy, EDS (JEOL 6460LV, FEI-Teneo, FEI, CITIUS) were performed on the eroded surfaces and on polished cross sections cut through the machined areas.

3. Results and discussion

3.1. Material removal rate and stability of the EDM process

Table 2 shows the results regarding EDM performance or efficiency in terms of material removal rate (MRR) and electrode wear rate (EWR) of each EDM process. The energy of each process is indicated, as well as some microstructural aspects characteristic of the composites (density and grain size). The electrical conductivity value for each composite (parallel and perpendicular to the sintering pressing axis) is also indicated, since this is a clue parameter which influences the EDM process.

It should be noticed that a high material removal rate in ceramics may correspond to a spalling mechanism, so it does not always indicate a better performance than moderate MRR values. Roughness parameters will be discussed in detail in Section 3.2.3.

Fig. 2 shows the morphology of the machined geometries as well as the angle between the bottom and lateral surfaces depending on EDM conditions. It can be seen that stronger deviations from 90° are obtained in the cases of e-GNP and FLG-based nanocomposites. In contrast, the materials filled with GNP showed lower lateral machining, with lesser material removal, which can lead to high accuracy for finishing processes. This fact can be attributed to the higher electrical conductivity of the first ones: $\sigma_{\perp}$ and $\sigma_{||}$ in the case of e-GNP-based materials, and $\sigma_{\perp}$ in the case of FLG-based nanocomposites.

The main result is that process stability is achieved in the three composites at low energy, so the three composites are ED-machinable. Focusing on the differences between the composites, the e-GNP composite is stable only for low energy, showing the worst performance in terms of EDM machinability and the GNP composite exhibits the best performance in terms of machinability since the process is stable for low and medium energy, and sufficient for high energy.

Table 2
Microstructural characteristics –density and grain size- and electrical conductivity of the studied composites. Efficiency parameters of each EDM process: material removal rate (MRR), electrode wear rate (EWR) and surface roughness (Ra). LE, ME and HE stand for low, medium and high energy, respectively, regarding the discharge current.

Material	Density [g/cm^3]	Grain size D planar (μm+- sd)	Electrical conductivity (S/m) x10^3	EDM Energy	MRR [mm^3/min]	EWR [%]	Ra (μm)
e-GNP	5.2	0.19±0.12	$\sigma_\perp$ **2.8**±0.2	LE	**0.94**	0.479	0.45±0.05
					0.91	1.395	0.34±0.04
			$\sigma_{\|\|}$ 1.67±0.11	ME	Unstable		1.5±0.4
					Unstable		0.95±0.12
GNP	5.3	0.14±0.06	$\sigma_\perp$ 2.7±0.2[18]	LE	**0.70**	1.175	1.5±0.5
			$\sigma_{\|\|}$ 0.54±0.02[18]		**0.73**	1.329	1.2±0.4
				ME	**1.79**	-0.501	1.0±0.3
				HE	***2.68****	0.056	0.7±0.3
FLG	5.0	0.29±0.16	$\sigma_\perp$ 4.1±0.3	LE	**1.06**	-1.336	0.7±0.3
			$\sigma_{\|\|}$ 0.30±0.02	ME	**2.20**	-0.340	0.7±0.3
				HE	unstable	-2.205	0.78±0.13

* Process not completely stable but sufficient

3.2. Microstructural characterization of the EDMed surfaces

3.2.1. Damage assessment of the graphene-based nanostructures on the EDMed surfaces

Raman spectroscopy is a powerful tool to analyze the possible damage of the composites EDMed surface, such as GBN amorphization or structural defects in the carbonaceous nanostructures. In this way, Raman spectra were acquired on the surfaces EDMed at low, medium and high energy of the three composites (Fig. 3).

For the three composites, the spectra acquired on the low energy EDMed surfaces showed the characteristic bands of graphitic species associated to GBN [14,18,19], i.e., D- (~1350 cm^{-1}), G- (~1590 cm^{-1}), and 2D-bands (~2700 cm^{-1}), with quite similar intensity ratios –I_D/I_G and I_{2D}/I_G– to the observed ones on the untested surfaces. This confirms that this EDM energy level is not altering the GBN structure in any of the composites.

When increasing the energy level to Medium, no significant differences in the Raman bands intensity ratios are observed for the GNP and FLG composites (Fig. 3(b) and (c)). However, the shape and I_D/I_G ratio in the spectra for the e-GNP composite are significantly altered (Fig. 3(a)). The D- and G-bands are remarkably broadened with high I_D/I_G, and a wide feature is observed between them, at ~1500 cm^{-1}. Moreover, the 2D-band is not present in the spectra. All this reveals that the e-GNP on the medium energy machined surface became highly damaged, and their structure present a high amount of structural defects and amorphous carbon [16].

The spectra acquired on the high energy EDMed surfaces of the GNP and FLG composites also present the characteristic features for highly damaged GBN: broadened D- and G-bands with high I_D/I_G, wide feature at ~1500 cm^{-1} and significantly lower I_{2D}/I_G ratio.

Therefore, the Raman spectra analysis indicates that the graphene in e-GNP composite turns amorphous at medium electric discharge energy, while in the case of GNP composites the graphene amorphization requires a high discharge energy. In the FLG composites there is a gradual shift towards amorphous, indicated by the disappearance of the peak at 2400 cm^{-1}. However, the absence of amorphous carbon in the Raman spectra cannot assure that it does not form. In the case of the e-GNP composites, the amorphous carbon can be easily detected. There is a significant amount of resolidified material, and the decomposition of graphene is evident because the material containing it is still attached to the surface (Fig. 4a). In the case of GNP and FLG composites up to medium energy, the resolidified layers are very thin (Fig. 4b, c and Fig. 5), so if the graphene in the process zone has become amorphous, it cannot be detected anymore since it has disappeared with the machining debris. In the case of high energy machined surfaces for GNP and FLG composites, there is a significant resolidified layer so the graphene decomposition can be inferred (Figs. 5 and 6).

The remarkable damage observed after medium energy EDM of the e-GNP composite, and after high energy EDM of the GNP and FLG composites can be related to the high temperatures achieved during EDM with severe testing conditions, as previously reported [7]. The fact that the e-GNP are damaged at a lower EDM energy level than the GNP and the FLG could be a consequence of the possible presence of structural defects introduced on their structure during the planetary ball milling process, as it has been previously suggested [15].

3.2.2. SEM characterization of the EDMed surfaces and cross sections

The EDMed surface of the three composites at low energy (corresponding to EDM stable processes) is shown in Fig. 4. The common features are a glassy melted surface with craters (circular voids). The craters are a consequence of the gasses that get entrapped inside granules of the workpiece material during the machining due to the high temperatures reached by the EDM process (6000–7000 °C) [20]. These granules break off when the discharge duration and the neat heat flux increase, allowing the entrapped gasses to escape. This leads to the formation of voids, which is an undesired effect [21]. The melted regions cover a great area percentage of the EDMed surfaces and present cracks, as reported by other authors in CNT/zirconia composites [7] or zirconia tungsten carbide composites [22]. The cracks on the melted layer, also a common feature in the three composites, are the result of residual stresses due to the rapid cooling after the EDM process.

The most striking difference observed in these EDMed surfaces in top view with respect to the literature is that there is no clear splat structure as in the case of metals or other ceramic composites such as TZP-WC [22]. This absence of splats could be a consequence of the machining direction. The composites in this study have been machined in the perpendicular direction to the SPS pressing direction and along the graphene main plane, while in the cases typically reported in the literature, the machining direction corresponds to the pressing direction.

Regarding the differences between the three composites' EDMed surface at low energy, in the GNP composite, the melted regions are smoother and cover larger areas. Sparse micron and submicron sized debris can be observed in the e-GNP composite (Fig. 4a). The light circles observed in FLG specimen are due to charge effects in the electron microscope, because the recast layers are much thinner.

The increase in EDM energy produces, in the three composites, an increase in the craters' diameter [9], as well as in the spalling and the surface roughness (see supplementary Figs. S1, S2 and S3). The melted layers also show larger and uneven thicknesses. The increase in the thickness of the recast layer has been correlated to an increase in the graphene content in GNP-SiC composites [23].

The composite with e-GNP presents craters up to 10 μm in diameter combined with small submicrometric shallow ones which give the medium-energy EDMed surface the appearance of a coral-like structure (Fig. 5c). The coral-like surface pattern or sponge-like aspect have only been observed on the e-GNP composite and can be attributed to the smaller lateral size of the e-GNP compared to the GNP and the FLG. The SEM micrographs of the EDMed surfaces at low and medium energy at

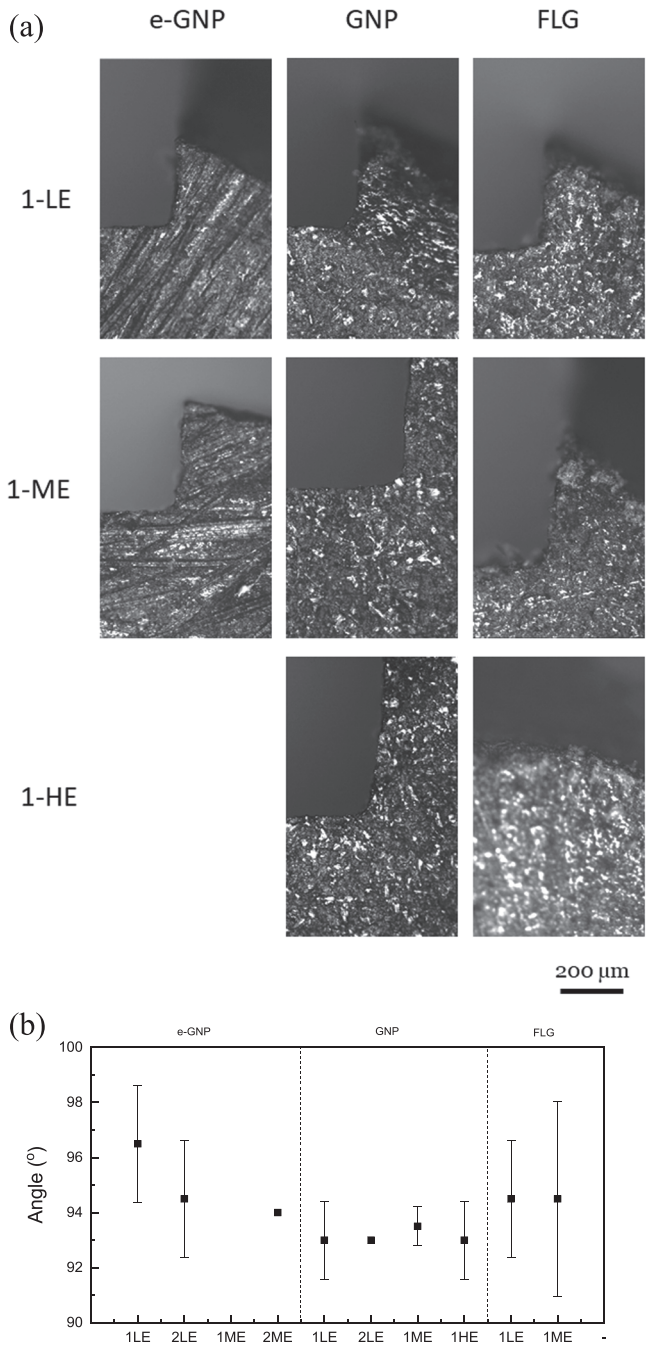

Fig. 2. (a) Optical micrographs showing the morphology of the machined samples and (b) angle between bottom and lateral generated surfaces.

different magnifications can be compared in supplementary Fig. S1.

The EDMed surface of the composite with GNP, in Fig. 6, shows similar features for the three conditions: low, medium and high EDM energy, although the high energy surface presents a higher fraction of melted region and more debris (Fig. 6b). This composite is therefore the most resistant to the different EDM energy levels, showing a better performance and machinability in terms of surface finish and EDM energy tolerance. The SEM micrographs of the EDMed surfaces at low, medium and high energy at different magnifications can be compared in supplementary Fig. S2.

The EDMed surfaces of the composite with FLG (Fig. 5b, d) exhibit also the typical melted regions with craters and cracks (usually connecting the craters). When the EDM energy increases, the melted areas become thicker, the debris content increase and the crystalline character of the melted areas becomes more evident (Fig. 5d). This crystalline character of the recast layer has also been reported in zirconia-based materials by Rapp et al. [22]. At high discharge energy, carbon nanotubes are clearly observed (Fig. 5b, d). The generation of carbon nanotubes due to arc discharges was first reported in the literature by Iijima [24]. The high EDM energy can degrade some FLG nanostructures from the surface and transform them into nanotubes, either directly or via amorphous carbon or even carbo-thermally formed ZrC. These nanotubes have not been detected in the other specimens, maybe due to the higher thickness of the GNP and the smaller lateral dimension of the e-GNP. The SEM micrographs of the EDMed surfaces at low, medium and high energy at different magnifications can be compared in supplementary Fig. S3.

The cross sections of the EDMed surfaces of the three composites at the different electrode energies can be observed and compared in Fig. 7. The EDMed cross sections of the e-GNP composite (Fig. 7a) present a very smooth surface in the case of low EDM energy, without any cracks. The melted recast layer can reach only up to ~2 µm depth which is the best result in terms of surface finish among all the samples tested in this work. This value is similar to published results in CNT/alumina composites [6]. However, when the EDM energy increases to medium level (unstable process), some ceramic zones without e-GNP appear near the surface (clean ceramic areas in Fig. 7b). This effect has been observed only in this e-GNP sample and can be the result of the smaller size of the e-GNP and the possible structural damage to the GBN caused by the highly energetic milling process, which make them more likely to burn when EDM energy increases. Another unusual effect noticed only in these medium energy EDMed samples are dendritic-like structures (see supplementary Fig. S4) with darker and lighter areas. However, EDX results do not show any difference in composition between these areas (not shown). The surface roughness in these samples increases noticeably and sub-surface cracks appear over 50 µm under the surface, exhibiting a damaged structure (Fig. 7b). The accumulation of resolidified material with cracks underneath indicates melting and spalling [25]. This is the worst behavior in terms of surface finish among the tested samples. Sub-surface cracks have also been reported by other authors in EDM of zirconia with low electrical conductivity [7,22,25].

The EDMed cross sections of composite with GNP are also very similar for the three EDM energy conditions (Fig. 7c, d and e), with a surface layer that can reach 10 µm in depth, and a roughness slightly higher than the one for the low energy e-GNP surface. The increase in surface roughness is due to the larger GNP dimensions. Large GNP areas are observed on the EDMed surfaces, which indicates that the GNP structures survive to the EDM process, in accordance with the Raman analysis.

The EDMed cross sections of the FLG composite (Fig. 7f, g and h) show a clearly increasing roughness with increasing EDM energy. This indicates that the FLG composites are very sensitive to EDM energy. While the sample EDMed at low energy presents a smooth surface with a very fine surface melted layer (Fig. 7f), the medium energy one shows a thicker melted layer with bubble like spherical formations (Fig. 7g), which could be also acceptable in terms of surface finish. The sample EDMed at high energy (unstable process) presents also sub-surface vertical cracks (perpendicular to the EDMed surface) which seem to be caused by the FLG, which are also oriented with their main plane perpendicular to the EDMed surface (Fig. 7h). However, a few sub-surface cracks parallel to the surface have also been observed just below the melted layer, similarly to the reported ones by Melk et al. [7].

In order to have a global picture of the behavior of these composites after EDM, some important facts can be highlighted from the SEM analysis. If we compare the EDMed surfaces in this study, we can extract some concluding remarks about the operating mechanisms and the role of the electrical and thermal conductivity in view of the anisotropy in the different microstructure of the composites. On the one hand, the surface structures of the e-GNP ceramics machined with higher energy show quite thick recast layers containing no visible graphene, spallation

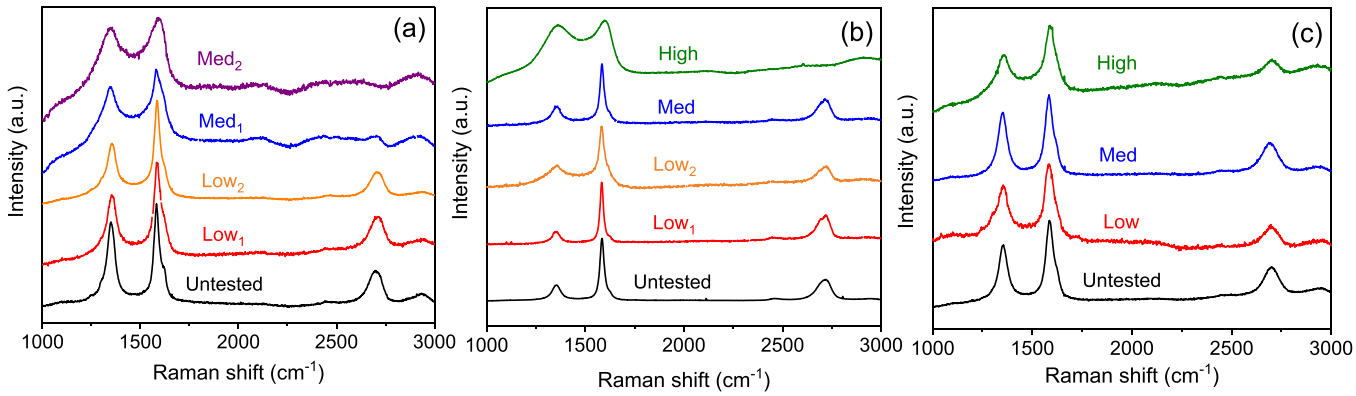

Fig. 3. Raman spectra acquired on the EDMed surfaces of the composites. (a) e-GNP, (b) GNP and (c) FLG. Spectra for the untested composites are included for comparison.

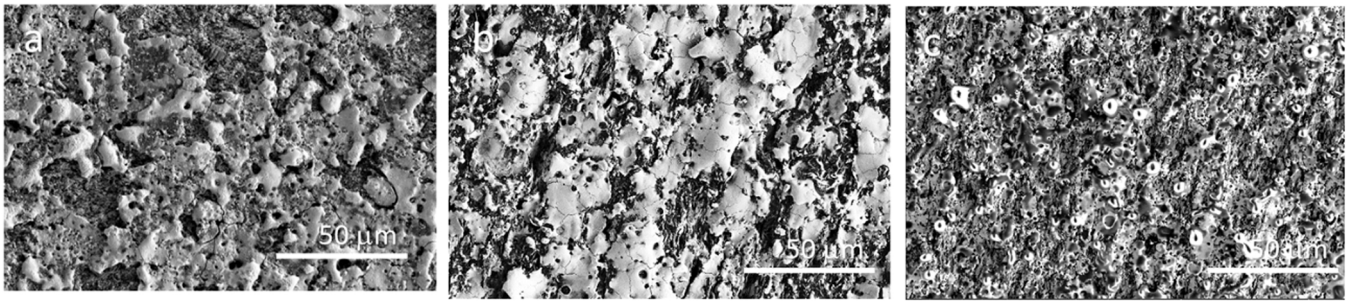

Fig. 4. SEM –SE of the EDMed surface of the composites with (a) e-GNP, (b) GNP and (c) FLG at low electrode energy corresponding to stable EDM processes.

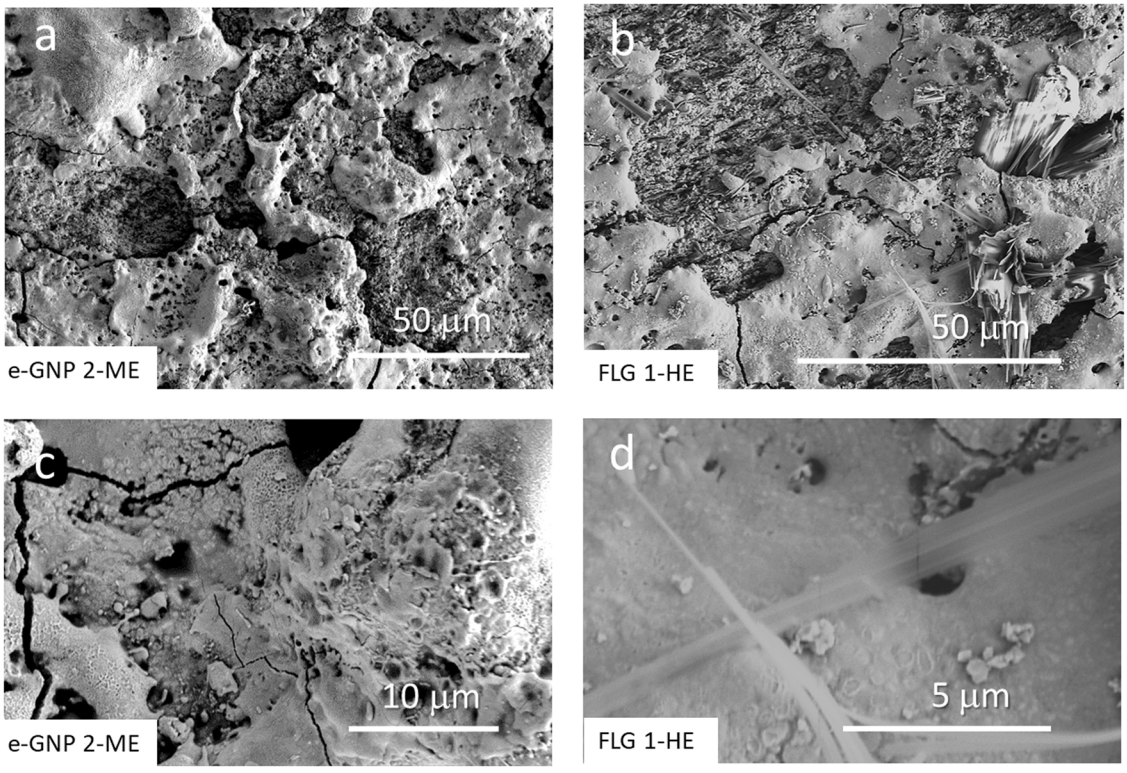

Fig. 5. SEM –SE of the EDMed surface of the composite with (a, c) e-GNP at medium energy and (b, d) FLG at high energy, all corresponding to unstable EDM processes.

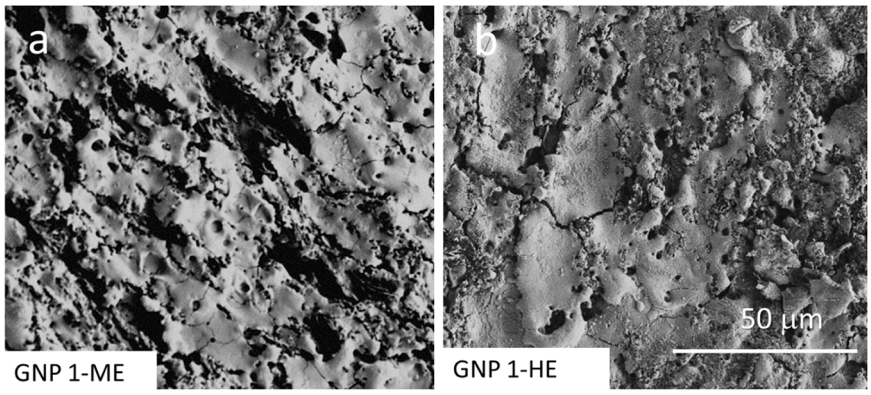

Fig. 6. SEM –SE of the EDMed surface of the composite with GNP at (a) medium and (b) high energy (corresponding to stable EDM processes).

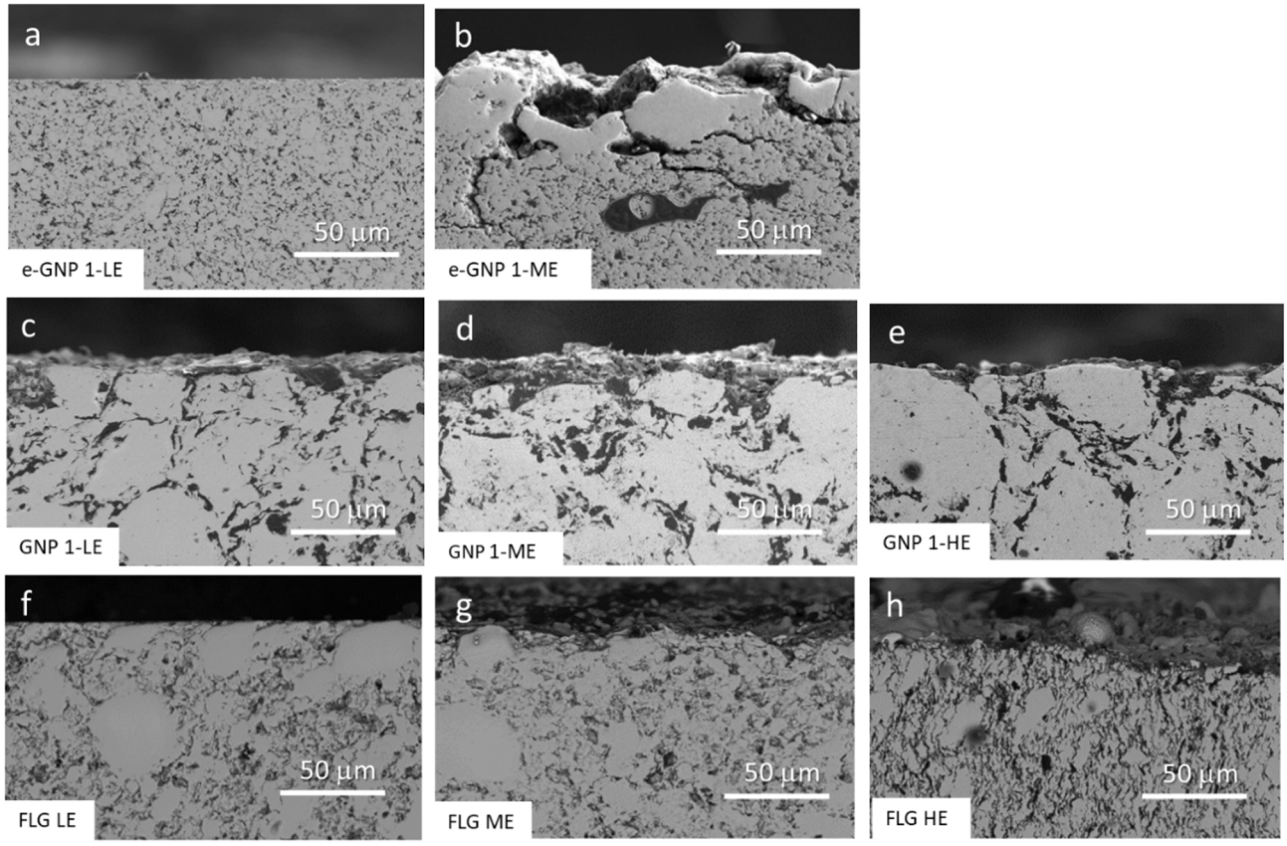

Fig. 7. SEM (with T1 detector) showing the cross sections of the EDMed surfaces of the three composites with different electrode energies. (b) and (h) correspond to unstable EDM processes.

and formation of perpendicular and lateral cracks. This may be a result of the more isotropic conductivity in these composites, which dissipate the discharge heat not only into the bulk (as happens in the other composites along the graphene platelets) but also in lateral direction. This implies that the temperatures achieved locally are high enough to melt the zirconia, so most of the melt re-solidifies and is not removed. These re-solidified layers (which apparently contain no graphene) are closely attached to the bulk material. The re-solidification is associated with shrinkage which induces spallation and the formation of cracks. This is probably promoted by the fact that the bulk contains a larger fraction of graphene based nanostructures and has a lower thermal expansion coefficient.

On the other hand, in the GNP and FLG composites the electrical conductivity -and therefore the thermal conductivity- are highly anisotropic, showing a high conductivity value in plane (in the machining direction) and a low conductivity out of plane (normal to the machining direction in this study). The recast layers are much thinner -especially in case of FLG at low energy- and it seems that the re-solidified melt easily spalls off or is just loosely attached to the bulk. The lower conductivity normal to the machining direction is likely to reduce the energy dissipation to the sides, producing a narrower heat affected zone and a higher temperature at the base of the discharges. This would cause a melt of lower viscosity which is removed and does not re-solidify, producing this thinner recast layers. However, in the case of the FLG-HE machining test (at high energy) probably due to the unstable process there is again a thicker resolidified layer with some cracks (Fig. 5b, d and Fig. 7h).

3.2.3. Surface roughness parameters of the EDMed composites

Surface finish and quality are key parameters in a wide range of applications as they can strongly influence the mechanical and tribological behavior of components as well as the performance of contact joints [26]. Fig. 8 shows representative 3D topographies of the EDMed surfaces for the three studied composites. For the e-GNP processed surfaces, the topography is homogeneous at low energy machining conditions. Nevertheless, when medium energies are used, the process became unstable, and some homogeneities emerge due to the already mentioned increase of craters' diameter (up to 25 μm) and spalling. Similar topographic morphologies are obtained in the case of the GNP and FLG composites, although inhomogeneities are more significant when the process starts to be unstable (high energies).

In order to elucidate quantitative differences obtained on profiles, 3D roughness parameters were evaluated. Fig. 9 shows the evolution of the maximum valley depth (Rv), maximum peak height (Rp), peak-peak height (Rz), surfaces kurtosis (Rku), surface skewness (Rsk), root mean squeare (Rq) and arithmetic mean roughness (Ra). A diminution in roughness parameters, compared to the surface of the unmachined sample, occurs for the EDMed surfaces of the e-GNP composite, being Ra below 0.5 μm. These values are lower than other reported data for micro-EDM milling of non-conductive zirconia [27] and make possible to use EDM as finish process [28]. When the process becomes unstable, a significant increase can be observed in all the calculated parameters, although Rku and Rsk remain mainly invariable, there is no increase in the asymmetry of the profile.

It is relevant to point out that the EDMed surfaces of this composite are considerably smoother than the ones on the other studied materials. This fact can be attributed to the smaller size of the e-GNP and the higher electrical conductivity ($\sigma_{||}$) exhibited by this composite (see Table 1), promoted by the isotropic electrical network created through the ceramic matrix, in contrast to the electrical anisotropy of GNP and FLG-based composites.

In contrast, the machined surfaces of the GNP composite showed higher roughness related values, which can be due, as mentioned, to the larger GNP dimensions. In this case, higher energies in the process, with the consequent augment of MRR, lead to lower roughness, diminishing Rv, Rp. Rp. Rsk, Ra and Rq. This is consequent with the larger melted regions observed by SEM when using higher machining energies.

In the case of the FLG composite, an increase of energy in the process caused an asymmetry in topograhy increase (Rsk) in the medium energy EDMed sample, due to the creation of bubble-like spherical formations (Fig. 7h) but it did not cause significant changes in surface roughness, which makes this composite attractive for EDM with medium electrode energy.

4. Conclusions

The three types of 3YTZP composites with 20 vol% graphene nanostructures studied are ED-machinable using a low electrode energy, which makes these materials good candidates for fabrication of high precision structural micro parts with complex shapes for different applications. This is supported by the stability of the EDM process, the preserved integrity of the graphene nanostructures and the geometrical tolerance maintained. The recast layers indicate melting mechanisms.

- The composite with small, exfoliated GNP, e-GNP, presented the best surface finish at low energy, due to the reduced size of the nanostructures, its homogeneous and isotropic microstructure, and the highest average electrical conductivity. However, it could not stand a stable EDM process nor microstructural preservation for medium electrode energy, due to the pre-existent structural defects of the e-GNP induced by ball milling.
- The composite with FLG presented the highest material removal rate value for medium electrode energy with undamaged FLG and a good surface finish. The low thickness of the few layer graphene may be responsible for the limited tolerance to increasing EDM energy.
- The composite with GNP exhibited the best EDM machinability with stable processes and a stable microstructure for low, medium and high energy. Besides, decreasing roughness with increasing electrode

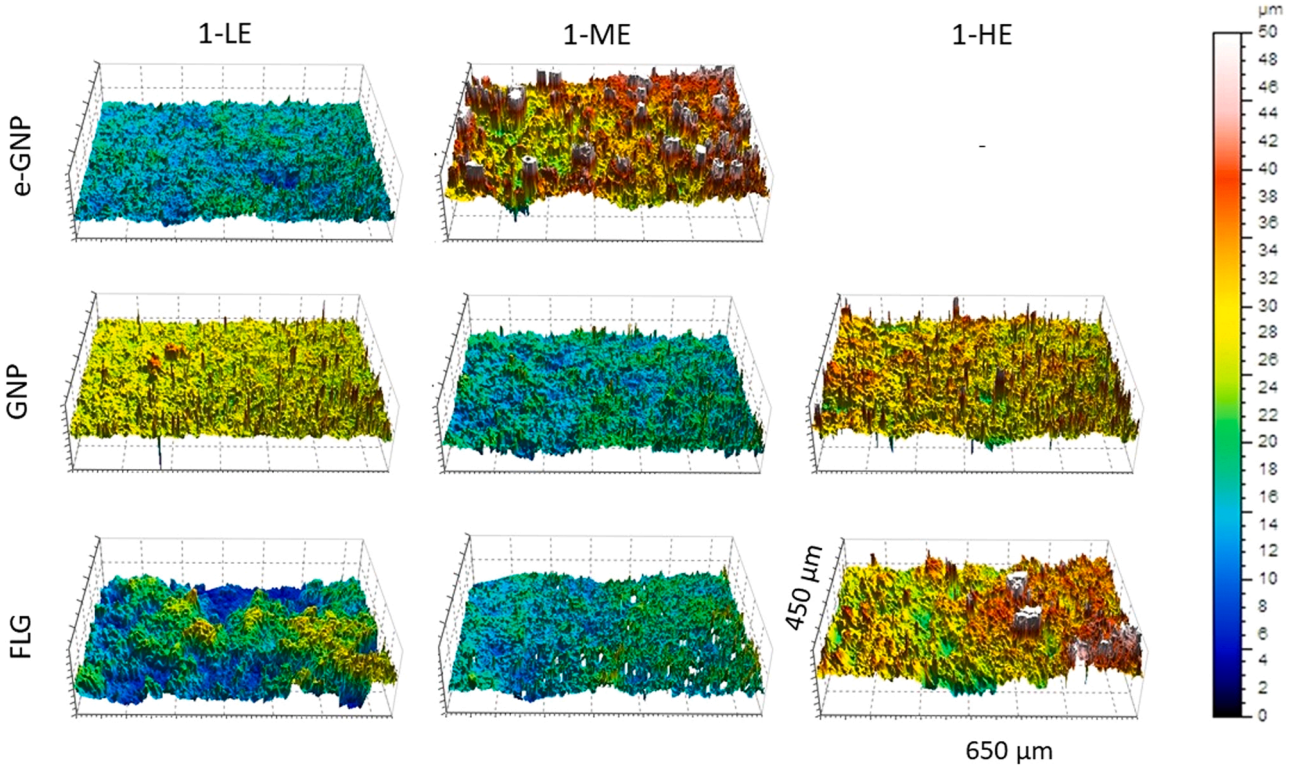

Fig. 8. Confocal 3D topography of the EDMed surfaces.

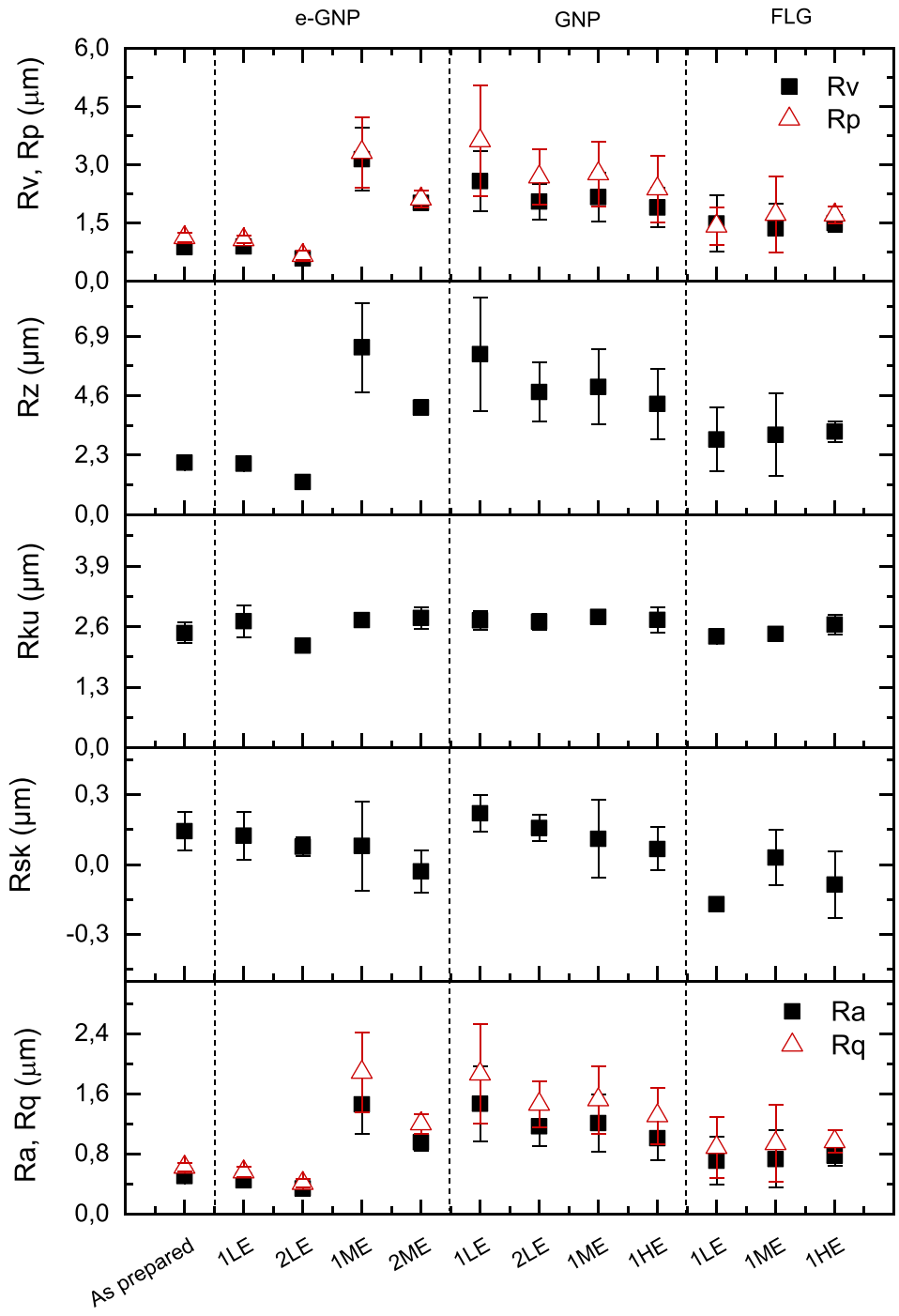

Fig. 9. Roughness parameters for the different EDMed surfaces.: maximum valley depth (Rv), maximum peak height (Rp), peak-peak height (Rz), surfaces kurtosis (Rku), surface skewness (Rsk), root mean squeare (Rq) and arithmetic mean roughness (Ra).

energy has been measured. The higher thickness and lateral size of the GNP used for this composite is beneficial for EDM.

Declaration of Competing Interest

The authors declare that they have no known competing financial interests or personal relationships that could have appeared to influence the work reported in this paper.

Acknowledgements

This research was supported by the projects PGC2018-101377-B-100 funded by MCIN/AEI/ 10.13039/501100011033 (Ministerio de Ciencia e Innovación, Spanish Government, Agencia Estatal de Investigación) and ERDF (European Regional Development Funding) "A way of making Europe", by the European Union and project P20_01024 (Junta de Andalucía/FEDER, UE 2014–2020). C. López-Pernía acknowledges the financial support of MINECO (Ministerio de Economía y Competitividad, Spanish Governmet) through the FPI contract ref: BES-2016- 078711. C.

Muñoz-Ferreiro acknowledges the financial support of a VI PPIT-US (Plan Propio Universidad de Sevilla, Spain) fellowship through the contract USE-18740-H. R. Moriche acknowledges the financial support of MINECO through the Juan de la Cierva Postdoctoctoral Program (FJCI-2017-32502).

Appendix A. Supporting information

Supplementary data associated with this article can be found in the online version at doi:10.1016/j.jeurceramsoc.2022.06.037.

References

[1] W. Ming, et al., A comprehensive review of electric discharge machining of advanced ceramics, Ceram. Int. vol. 46 (2020) 21813–21838.
[2] A. Bilal, M. Jahan, D. Talamona, A. Perveen, Electro-discharge machining of ceramics: a review, Micromachines 10 (2018) 10.
[3] A. Gommeringer, C. Schweizer, F. Kern, R. Gadow, Electrical discharge machinable (Y, Nd) co-stabilized zirconia – Niobium carbide ceramics, J. Eur. Ceram. Soc. 40 (2020) 3723–3732.
[4] A. Gommeringer, et al., ED-machinable ceramics with oxide matrix: influence of particle size and volume fraction of the electrical conductive phase on the mechanical and electrical properties and the edm characteristics, Procedia CIRP 68 (2018) 22–27.
[5] A. Lazar, T. Kosmač, J. Zavašnik, A. Abram, A. Kocjan, TiN-nanoparticulate-reinforced ZrO2 for electrical discharge machining, Materials (2019) 2789.
[6] M.A. Singh, D.K. Sarma, O. Hanzel, J. Sedláček, P. Šajgalík, Machinability analysis of multi walled carbon nanotubes filled alumina composites in wire electrical discharge machining process, J. Eur. Ceram. Soc. 37 (2017) 3107–3114.
[7] L. Melk, M.L. Antti, M. Anglada, Material removal mechanisms by EDM of zirconia reinforced MWCNT nanocomposites, Ceram. Int. 42 (2016) 5792–5801.
[8] D. Hanaoka, et al., Electrical discharge machining of ceramic/carbon nanostructure composites. in, in: Procedia CIRP, vol. 6, Elsevier B.V,, 2013, pp. 95–100.
[9] O. Malek, et al., Carbon nanofillers for machining insulating ceramics, Mater. Today 14 (2011) 496–501.
[10] F. Zeller, C. Müller, P. Miranzo, M. Belmonte, Exceptional micromachining performance of silicon carbide ceramics by adding graphene nanoplatelets, J. Eur. Ceram. Soc. 37 (2017) 3813–3821.
[11] J.-W. Sung, K.-H. Kim, M.-C. Kang, Effects of graphene nanoplatelet contents on material and machining properties of GNP-dispersed Al2O3 ceramics for micro-electric discharge machining, Int. J. Precis. Eng. Manuf. Technol. 3 (2016) 247–252.
[12] Y. Tan, H. Luo, H. Zhang, S. Peng, Graphene nanoplatelet reinforced boron carbide composites with high electrical and thermal conductivity, J. Eur. Ceram. Soc. 36 (2016) 2679–2687.
[13] N. Obradović, F. Kern, Properties of 3Y-TZP zirconia ceramics with graphene addition obtained by spark plasma sintering, Ceram. Int. 44 (2018) 16931–16936.
[14] A. Gallardo-López, I. Márquez-Abril, A. Morales-Rodríguez, A. Muñoz, R. Poyato, Dense graphene nanoplatelet/yttria tetragonal zirconia composites: Processing, hardness and electrical conductivity, Ceram. Int. 43 (2017) 11743–11752.
[15] C. López-Pernía, et al., Optimizing the homogenization technique for graphene nanoplatelet/yttria tetragonal zirconia composites: Influence on the microstructure and the electrical conductivity, J. Alloy. Compd. 767 (2018) 994–1002.
[16] C. Muñoz-Ferreiro, C. López-Pernía, Á. Gallardo-López, R. Poyato, Unravelling the optimization of few-layer graphene crystallinity and electrical conductivity in ceramic composites by Raman spectroscopy, J. Eur. Ceram. Soc. 41 (2021) 290–298.
[17] Á. Gallardo-López, et al., Spark plasma sintered zirconia ceramic composites with graphene-based nanostructures, Ceramics 1 (2018) 153–164.
[18] C. Muñoz-Ferreiro, et al., Microstructure, interfaces and properties of 3YTZP ceramic composites with 10 and 20 vol% different graphene-based nanostructures as fillers, J. Alloy. Compd. 777 (2019).
[19] A.C. Ferrari, D.M. Basko, Raman spectroscopy as a versatile tool for studying the properties of graphene, Nat. Nanotechnol. 8 (2013) 235–246.
[20] M. Kunieda, B. Lauwers, K.P. Rajurkar, B.M. Schumacher, Advancing EDM through fundamental insight into the process, CIRP Ann. - Manuf. Technol. 54 (2005) 64–87.
[21] M.A. Singh, D.K. Sarma, O. Hanzel, J. Sedláček, P. Šajgalík, Wire electrical discharge machining of MWCNT filled alumina composites, in: Materials Today: Proceedings, vol. 5, Elsevier Ltd,, 2018, pp. 5722–5726.
[22] M. Rapp, A. Gommeringer, F. Kern, Electrical discharge machinable ytterbia samaria co-stabilized zirconia tungsten carbide composites, Ceramics 4 (2021) 408–420.
[23] O. Hanzel, M.A. Singh, D. Marla, R. Sedlák, P. Šajgalík, Wire electrical discharge machinable SiC with GNPs and GO as the electrically conducting filler, J. Eur. Ceram. Soc. 39 (2019) 2626–2633.
[24] S. Iijima, Helical microtubules of graphitic carbon, Nature 354 (1991) 56–58.
[25] T. Bergs, M. Olivier, A. Gommeringer, F. Kern, A. Klink, Surface Integrity Analysis of Ceramics Machined by Wire EDM Using Different Trim Cut Technologies, in: Procedia CIRP, vol. 87, Elsevier B.V,, 2020, pp. 251–256.
[26] D.M. Shivanna, M.B. Kiran, S.D. Kavitha, Evaluation of 3D surface roughness parameters of EDM components using vision system, Procedia Mater. Sci. 5 (2014) 2132–2141.
[27] A. Schubert, H. Zeidler, M. Hahn, M. Hackert-Oschätzchen, J. Schneider, Micro-EDM milling of electrically nonconducting zirconia ceramics, Procedia CIRP 6 (2013) 297–302.
[28] M. Hadad, L.Q. Bui, C.T. Nguyen, Experimental investigation of the effects of tool initial surface roughness on the electrical discharge machining (EDM) performance, Int. J. Adv. Manuf. Technol. 95 (2018) 2093–2104.